Hollow chitosan–silica nanospheres as pH-sensitive targeted delivery carriers in breast cancer therapy

Ziwei Deng [a,1], Zipeng Zhen [b,1], Xiaoxi Hu [a], Shuilin Wu [a,c], Zushun Xu [a,c,*], Paul K. Chu [c,**]

[a] Ministry of Education Key Laboratory for the Green Preparation and Application of Functional Materials, Hubei University, Wuhan 430062, China
[b] Institute of Physical Education, Linyi University, Linyi, Shandong 276005, China
[c] Department of Physics & Materials Science, City University of Hong Kong, Tat Chee Avenue, Kowloon, Hong Kong, China

ARTICLE INFO

ABSTRACT

Promising drug nanocarriers consisting of mono-dispersed and pH sensitive chitosan–silica hollow nanospheres (CS–SiO$_2$ HNPs) suitable for breast cancer therapy are produced and investigated. The SiO$_2$ HNPs are fabricated using a one-step, one-medium process which obviates the need for post-treatment to remove the templates, additional dissolution, or calcination. Taking advantage of the cross-linking reaction with (3-Glycidyloxypropyl) trimethoxysilane (GTPMS), cationic polysaccharide-chitosan decorates the surface and produces pH sensitive CS–SiO$_2$ HNPs. The materials enable controlled release of loaded drugs in pericellular and interstitial environments. In particular, the antibody molecule (to ErbB 2) can be conjugated onto the surface of the CS–SiO$_2$ HNPs thereby allowing the hollow nanospheres to serve as a targeted delivery agent to breast cancer cells. TNF-α are delivered to MCF-7 breast cancer cells under both *in vitro* and *in vivo* conditions to suppress the growth of cancerous cells and even kill them with high therapeutic efficacy. Owing to their hollow inner cavity and porous structures, the CS–SiO$_2$ HNPs are excellent pH-responsive targeted nanocarriers.

1. Introduction

Nano-medicine has enormous potential and may revolutionize disease diagnosis and therapy [1–5]. Recently, organic and/or inorganic nanomaterials such as liposomes, polymersomes, micelles, dendrimers, carbon-based materials, gold-based materials, iron oxide, silicon, and some semiconductors with various morphologies including quantum dots, nanocapsules, nanotubes, and nanocages have been fabricated and explored as new platforms for diagnostic and therapeutic purposes [5–12]. Among the various nanomaterials, hollow silica nanoparticles with mesoporous structures are particularly attractive due to their large surface area, highly accessible pores, bio-inertness, and compatible properties and have been investigated as efficacious drug delivery carriers for small drug molecules, genes, and proteins [13–21].

A number of fabrication processes such as the nozzle reactor approach [22], heterophase polymerization combined with the sol–gel process [23–25], layer-by-layer self-assembly [26], and so on have been adopted for the preparation of hollow spheres comprising polymeric and/or siliceous materials, but these processes tend to be time consuming and complicated. For instance, multiple steps including surface functionalization of the template spheres, solvent exchange, and coating reactions are typically required to obtain the core-shell composite particles [23–25]. Post-treatment processes including organic solvent dissolution or calcination at elevated temperature are needed to remove the core particles in order to produce hollow spheres [26] consequently hampering wider biomedical applications. Therefore, a simple method to prepare hollow SiO$_2$ nanospheres is necessary in order to develop a new generation of drug delivery system for nanomedicine, disease diagnosis, and therapy. We have demonstrated that mono-dispersed SiO$_2$ HNPs can be fabricated via a one-step process. The formation of SiO$_2$ nanoshells and dissolution of polystyrene core particles occur in the same medium without post-treatment to remove the templates [27]. Considering the desirable characteristics such as unique hollow and porous structures and ease of surface functionalization, the materials have great potential as drug delivery carriers in cancer therapy. However, in order to enhance the

therapeutic efficacy and achieve fast drug release to selected sites and slow or zero drug release before reaching the targeted sites so as to minimize toxic side effects of anticancer drugs, the SiO_2 HNPs need to be conjugated with specific ligands or antibodies and incorporated into biomaterials responsive to external stimulation (pH or ion-sensitive). If this can be realized, the materials will be highly desirable in clinical applications [1,3,28,29].

Chitosan which is a natural cationic polysaccharide composed by β-(1-4)-linked glucosamine units together with some *N*-acetyl-D-glucosamine units is obtained by exhaustive deacetylation of chitin [30]. Owing to the favorable biodegradable, nontoxic, and antimicrobial properties, it has been used in different biomedical and drug delivery applications [31,32]. The amino groups in chitosan are protonated at a certain pH range and so chitosan can be responsive to external pH stimulation. As the pKa of chitosan is ~6.3, its pH response is near or slightly acidic. It has been reported that the microenvironment inside solid tumors has an acidic pH of 5—6.8 at which tumors have a lower extracellular pH than normal tissues [33—35]. Hence, chitosan is a promising biopolymer to provide SiO_2 HNPs with a pH responsive polyelectrolyte layer to control the release of loaded anticancer drugs to the acidic local environment in tumor tissues.

In this paper, we report a one-step method to fabricate monodispersed SiO_2 HNPs and then decorate them with chitosan using the cross-linking reaction with (3-Glycidyloxypropyl) trimethoxysilane (GTPMS). The resulting SiO_2 HNPs with a pH-sensitive polyelectrolyte layer are conjugated to the antibody molecule (to ErbB 2) to produce the desired nanocarriers for targeted TNF-α drug delivery to tumor cells.

2. Experimental section

2.1. Materials

Polyvinylpyrrolidone (PVP, MW = 40,000) and chitosan (CS, Medium molecular weight) with deacetylation of 75—85% and (3-Glycidyloxypropyl) trimethoxysilane (GPTMS) were purchased from Sigma—Aldrich and used without further purification. α,α'-azodiisobutyramidine dihydrochloride (AIBA) were supplied by Fluka (USA) and used as received. Styrene was bought from Shanghai Chemical Reagent Co. (China) and distilled to remove the inhibitor in vacuum and stored at 4 °C until use. Tetraethoxysilane (TEOS), absolute ethanol, aqueous ammonia (28 wt%), and acetic acid were purchased from Shanghai Chemical Reagent Co. (China). All chemicals were analytical grade and used as received without further purification. The phosphate buffered saline (PBS, 0.01 M, pH = 7.4) was prepared according to the documented procedures. Other buffers and media were purchased from Invitrogen
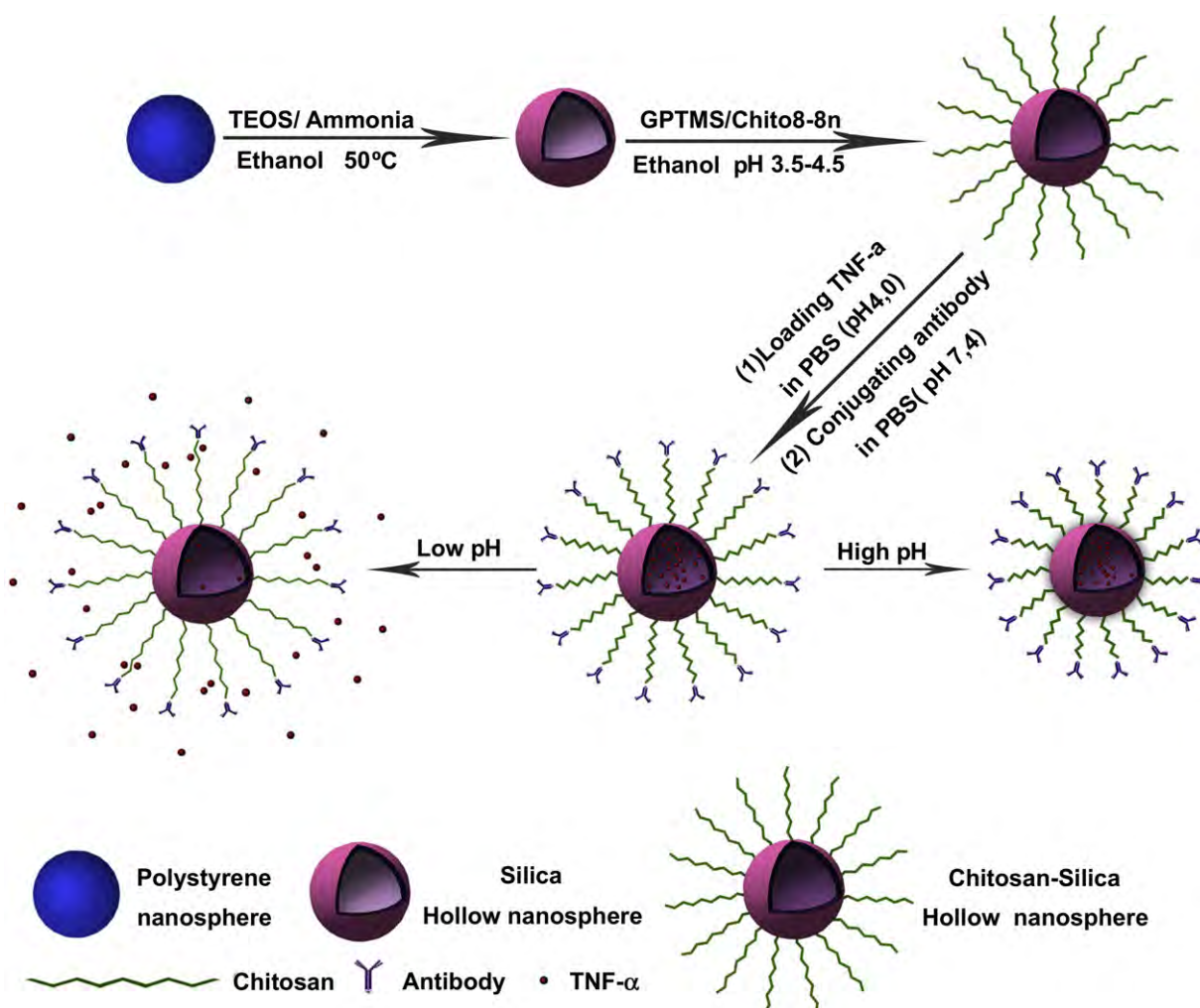
Scheme 1. Schematic diagram illustrating the formation of nanocarriers (CS—SiO₂-TNF-α conjugated with antibody) and the drug release behavior at different pH values. When the pH is low, the chitosan polymer chains swell in the medium opening the pores of the nanocarriers so that the loaded drugs can be easily released from the nanocarriers. On the contrary, at a high pH, the chitosan polymer chains are deprotonated and collapse to form a shield layer on the porous surface on the nanocarriers. This blocks and restricts drugs release from the hollow interior.
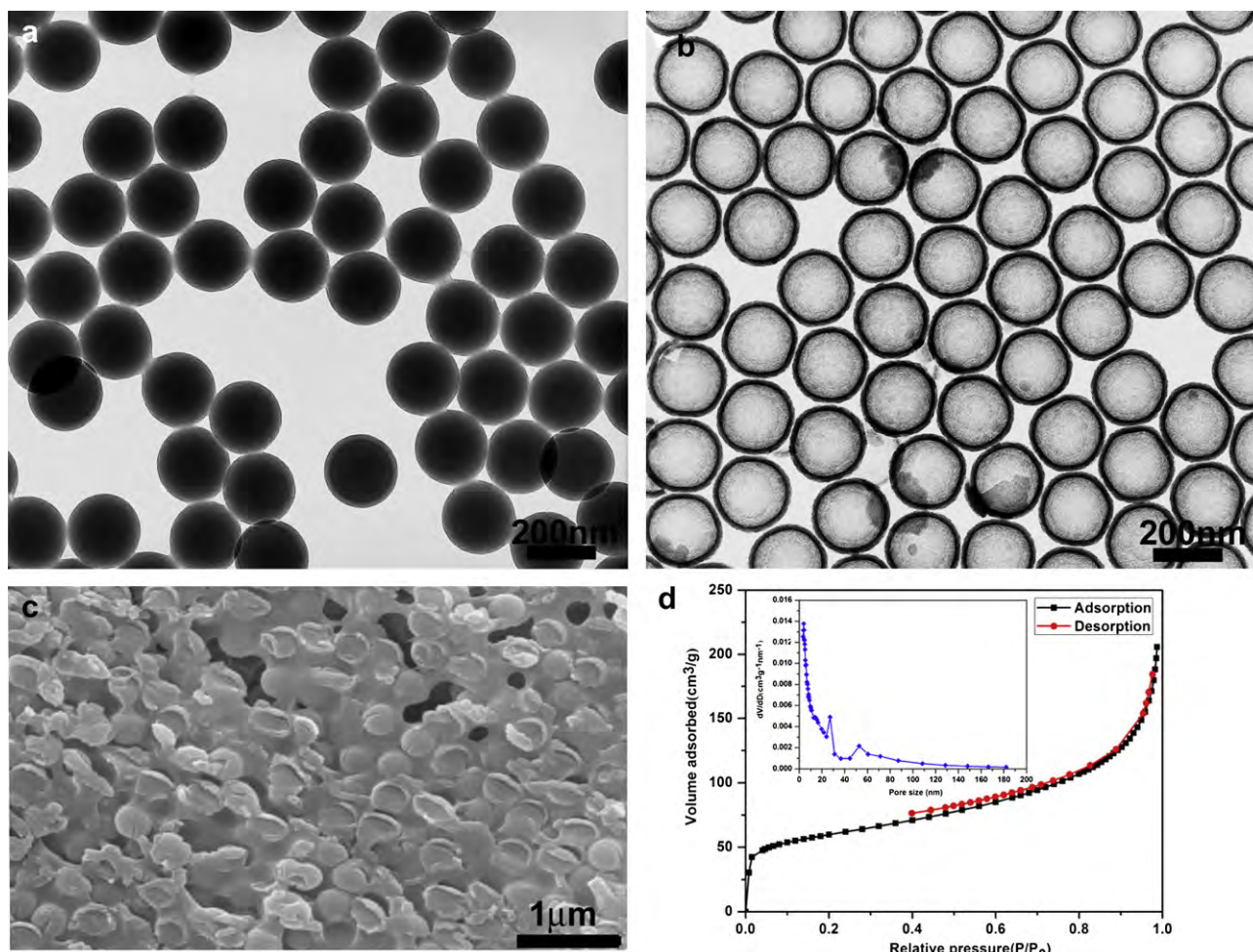
Fig. 1. TEM images: (a) Cationic polystyrene (PS) nanospheres obtained by emulsifier-free emulsion polymerization, (b) SiO₂ HNPs formed by sol−gel reaction between TEOS and PS in an ammonia/ethanol medium, (c) SEM images of the broken SiO₂ HNPs obtained from the ultrathin sections, and (d) nitrogen adsorption−desorption isotherm and Barrett−Joyner−Halenda (BJH) pore size distribution curves (inset) of SiO₂ HNPs.

Corp. Ultrapure water (resistivity > 17 MΩ cm⁻¹) produced by a Milli-Q water system was used in all the experiments.

2.2. Preparation of SiO₂ HNPs

The mono-dispersed cationic polystyrene (PS) nanospheres were prepared by emulsifier-free emulsion polymerization. Styrene (10.0 g), PVP (1.5 g), AIBA (0.26 g), and H₂O (100.0 g) were put into a 250 mL four-neck round-bottom flask with a mechanical stirrer, thermometer with a temperature controller, N₂ inlet, Graham condenser, and heating mantle. The solution was deoxygenated by bubbling nitrogen gas at room temperature for 60 min and then reacted at 70 °C for 24 h at the stirring rate of 100 rpm. A dialysis process was performed in ethanol using a cellulose membrane, and then the solid content in the cationic PS dispersion was tailored by the addition of ethanol. These mono-dispersed cationic PS nanospheres were used as templates to prepare the SiO₂ HNPs. TEOS (1.0 g), ammonia (5 mL), and ethanol (40 mL) were added to 5.0 g of the cationic PS dispersion and the sol−gel reaction proceeded at 50 °C for 1.5 h to produce the SiO₂ HNPs [27]. The SiO₂ HNPs was then collected by centrifugation, cleaned in deionized water and absolute ethanol ultrasonically several times, and then dried in a vacuum oven at room temperature for 24 h.

2.3. Preparation of CS−SiO₂ HNPs

The procedures to prepare the CS−SiO₂ HNPs were modified from previously reported protocols [32,36] and illustrated in Scheme 1. Chitosan (1.0 g) was dissolved in 200 mL of aqueous 3 wt% acetic acid to form a transparent chitosan solution (0.5% w/v), magnetically stirred at room temperature for 24 h, and filtered. The SiO₂ HNPs (10 mg) were dispersed in 5 mL of absolute ethanol ultrasonically for 15 min followed by addition of acetic acid to make the pH 3.5−4.5. (3-Glycidyloxypropyl) trimethoxysilane (GPTMS) (0.1 g) was then quickly injected into the SiO₂ dispersion and stirred at room temperature for 3 h. Afterward, 5 mL of the chitosan solution was introduced to the mixture and stirred at room temperature for 24 h to obtain the CS−SiO₂ HNPs. The final samples were collected by centrifugation (7000 rpm) followed by washing with excess deionized water and ethanol several times before freeze drying.

2.4. BSA protein drug loading and release from CS−SiO₂ HNPs

Bovine serum albumin (BSA) as one model protein drug was encapsulated onto the CS−SiO₂ HNPs to study the in vitro release in the PBS buffer solution under different pH condition. The CS−SiO₂ HNPs (10 mg) were added to 5 mL of the PBS buffer solution (pH 4.0) containing BSA (5 mg) and the mixture was stirred for two days. After addition of NaOH (0.2 M) to adjust the pH to 9.0, the chitosan polymer chains in the CS−SiO₂ HNPs were deprotonated and collapsed quickly under the basic conditions to form the shielding layers on the porous surface of the SiO₂ HNPs. This closed the pores and kept the loaded BSA inside the CS−SiO₂ HNPs. Afterward, the CS−SiO₂ HNPs loaded with BSA were centrifuged at 8000 rpm for 15 min. Finally, the supernatant was decanted and the BSA loaded samples were washed several times with the PBS buffer solution (pH 9.0).

The in vitro release procedures for BSA from the CS−SiO₂ HNPs were adopted from previously reported protocols [12,37]. Before BSA release, the BSA loaded CS−SiO₂ HNPs were dispersed and agitated in 5 mL of the PBS buffer solution at different pH values. The solution was centrifuged at 8000 rpm for 15 min, and 0.5 mL of the release medium was taken from the supernatant periodically. Another 0.5 mL of the fresh PBS medium was added to the solution to keep a constant volume after each sampling. As the BSA protein integrity had not been damaged during the loading procedures and after release from the hollow CS−SiO₂ HNPs, the concentration of released BSA could be determined by ultraviolet−visible (UV−vis) spectrophotometry [12] and all the release results were averages of five measurements.

2.5. In vitro TNF-α loading and antibody conjugating with CS−SiO₂ HNPs

TNF-α (Tumor Necrosis Factor α) which was reported to suppress the growth of MCF-7 breast cancer cells [38−40] was loaded onto the CS−SiO₂ HNPs for further
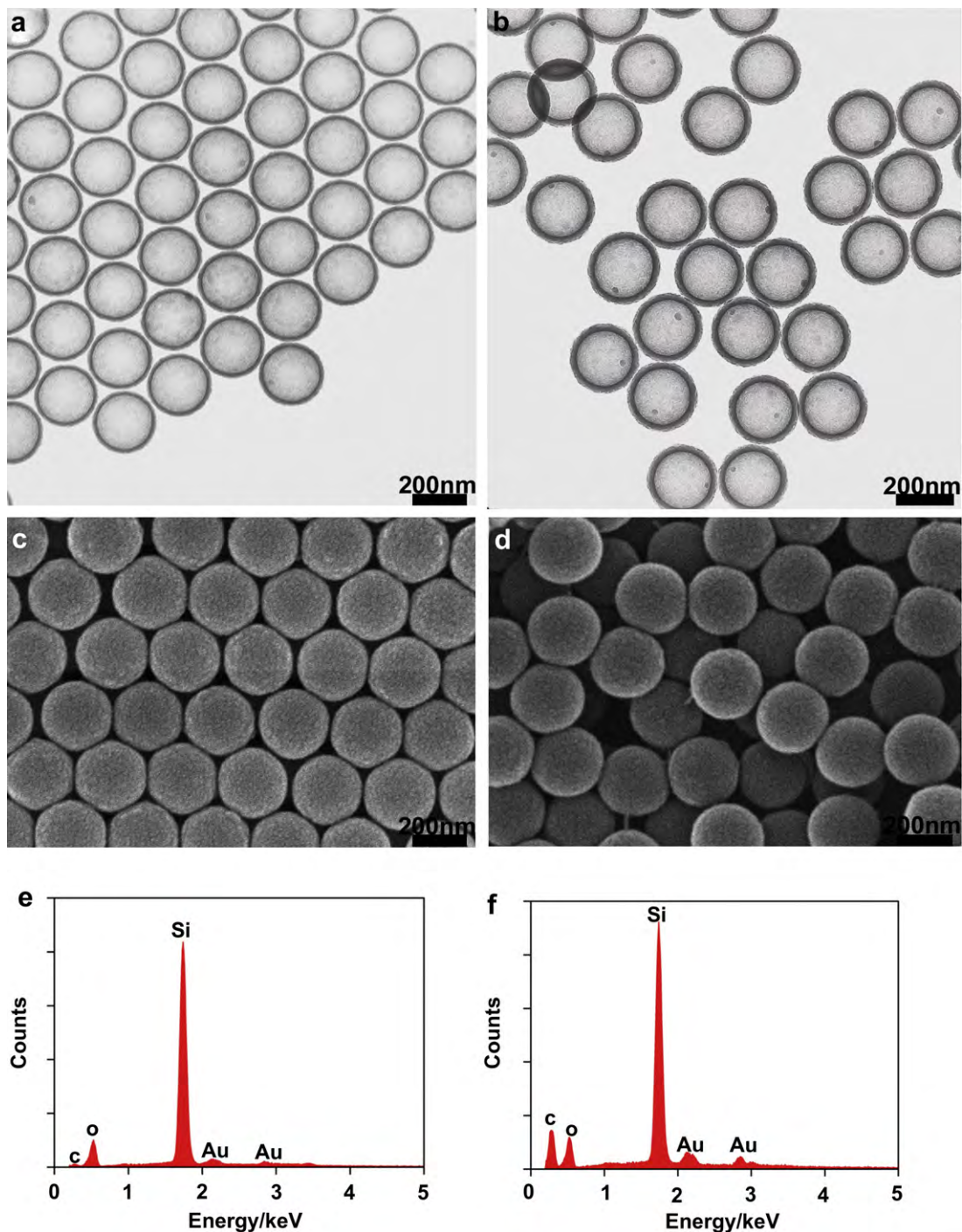
Fig. 2. TEM and SEM images of (a, c) SiO_2 HNPs and (b, d) CS–SiO_2 HNPs; EDS spectra of (e) SiO_2 HNPs and (f) CS–SiO_2 HNPs.

investigation. The CS–SiO_2 HNPs (10 mg) were first mixed with 5 mL of TNF-α in the PBS buffer solution (5 μg/mL, pH 4.0) (TNF-α was supplied by Boster Bioengineering, Wuhan, China). After stirring in an ice bath for 48 h, NaOH solution (0.2 M) was added to adjust the pH to 9.0. The TNF-α-loaded CS–SiO_2 HNPs (CS–SiO_2-TNF-α) were obtained by centrifugation and washed with the PBS buffer solution (pH 9.0). The CS–SiO_2-TNF-α were added to 5 mL of fresh PBS buffer solution (pH 7.4), cooled quickly, and refrigerated at -20 °C before use.

The antibody (to ErbB 2, ab2428) was purchased from Abcam, and 4.5 μg/mL of the antibody in the PBS buffer solution (pH = 7.4) was freshly prepared and directly used for the CS–SiO_2-TNF-α in the PBS buffer solution (pH = 7.4). Incubation proceeded in a tube at 18–20 °C under shaking for 2 h. Afterward, the mixture of the antibody conjugated to the CS–SiO_2-TNF-α in PBS solution (pH = 7.4) was stirred in an ice bath for several hours. Owing to the functional amino groups in the chitosan layers of CS–SiO_2 HNPs, they interacted with the carboxyl terminal end of the

antibody during the coupling process [41,42]. Following antibody immobilization, the CS–SiO_2-TNF-α conjugated with the antibody was separated by centrifugation, washed with the PBS buffer solution (pH 9.0), dispersed in 5 mL of fresh PBS buffer solution (pH 7.4), and refrigerated at -20 °C for subsequent *in vitro* and *in vivo* targeted delivery experiments.

2.6. MCF-7 cell culture

The MCF-7 breast cancer cells (bought from ATCC) were grown in the complete Dulbecco's modified Eagle's Medium/Ham's Nutrient Mixture F-12 (1:1; D-MEM/F-12, ATCC) strengthened with 10% (v/v) fetal bovine serum (FBS), 100 U/mL penicillin, and 0.1 mg/mL streptomycin and incubated under a humidified atmosphere of 5% CO_2 at 37 °C. The medium was changed once every three days. One week later, the cells were treated with trypsin/EDTA and washed with the PBS buffer solution (pH

Table 1
Hydrodynamic diameter and zeta potential of PS, SiO₂ HNPs and CS–SiO₂ HNPs under different pH conditions.

Samples	Hydrodynamic diameter [a](nm)			Zeta Potential [b](mV)		
	pH: 4.0	6.0	7.4	pH: 4.0	6.0	7.4
PS	222.5 ± 2.5	219.7 ± 2.8	218.9 ± 1.5	$+48 \pm 2.8$	$+26 \pm 1.6$	$+22 \pm 2.0$
SiO₂ HNPs	244.4 ± 1.6	242.8 ± 3.8	239.9 ± 2.9	-26 ± 2.5	-35 ± 2.1	-43 ± 2.3
CS–SiO₂ HNPs	345.6 ± 4.8	263.7 ± 3.7	252.3 ± 2.7	$+47.7 \pm 3.6$	$+24.7 \pm 2.9$	$+10 \pm 2.8$

All the values are reported as means with standard deviations.
 [a] Hydrodynamic diameters are measured at pH values of 4.0, 6.0 and 7.4 by DLS at room temperature.
 [b] Zeta potentials are measured at pH values of 4.0, 6.0 and 7.4 at room temperature.

7.4) for 3–5 min. The complete medium was also used to block the enzyme and then the cells were resuspended by centrifugation at 1000 rpm for 5 min. The cell number was counted using hemacytometer (Bio-equip) under an inverted microscope (Olympus) and the cell viability was determined by Typan Blue staining.

2.7. In vitro cytotoxicity and cell viability evaluation

The cell viability was determined from the MCF-7 cells. The cytotoxicity of pure CS–SiO₂ HNPs and CS–SiO₂-TNF-α at different concentrations or different incubation time was evaluated by the MTT (3-(4, 5-dimethyl thiazol-2-yl)-2, 5-diphenyl tetrazolium bromide) assay. The cells were plated at a density of 4×10^3 cells/well in 96-well plates in a standard growth medium for 24 h prior to exposure to the above materials. The cells were incubated in the growth medium containing different concentrations of pure CS–SiO₂ HNPs, or CS–SiO₂-TNF-α for 48 h at 37 °C. To evaluate how the drug release affected the cell viability, the cells were also treated by the same amount of CS–SiO₂-TNF-α for different incubation time. Meanwhile, wells containing only the cell medium were also prepared as untreated controls. After the treatment, MTT was used as an indicator of cell viability as determined by the mitochondrial-dependent reduction to formazane. MTT (5 mg/mL, 20 μL/well, Sigma, USA) was then added to the cell cultures for another 4 h at 37 °C. The supernatant was discarded, followed by addition of dimethyl sulfoxide (DMSO, 150 μL/well, Sigma, USA) and agitation for 20 s to completely dissolve the crystals. The absorbance of each well was measured at a wavelength of 490 nm by a microplate reader (BMG). The experimental results were expressed as mean values of three measurements and the cell viability was calculated by the following formula:

$$\text{Cell viability}(\%) = OD_{490}(\text{sample})/OD_{490}(\text{control}) \times 100,$$

where $OD_{490(\text{sample})}$ is the optical density (OD) of the treated cells measured at a wavelength of 490 nm and $OD_{490(\text{control})}$ represents that of the untreated control cells.

2.8. In vitro assay of killing efficacy

MCF-7 breast cancer cells (2×10^3) were seeded in six-well plates (ATCC) and the medium was refreshed after 24 h. CS–SiO₂-TNF-α conjugated to the antibody (200 μg/mL of CS–SiO₂ HNPs loaded with about 500 ng/mL of TNF-α) as the drug

delivery nanocarriers were added to the wells to treat MCF-7 cells and PBS (pH 7.4) was the control agent. 50 nM of acridine orange (AO, Boster) and 300 nM of propidium iodide (PI, Boster) were then added to the wells. After incubation for different time periods of 0 h, 6 h, 12 h, 24 h, 48 h, 72 h, and 96 h, inverted fluorescence microscopy (Olympus IX71) was employed to observe the plates. The killing efficiency of MCF-7 breast cancer cells treated with the drug nanocarriers at different concentrations from 50 to 400 μg/mL and consecutive time points were also determined by inverted fluorescence microscopy under the same conditions.

2.9. In vitro targeting verification

The MCF-7 breast cancer cells were incubated according to the aforementioned standard conditions. Before the cells were seeded, all the slides in the wells were treated according to the following procedures. They first underwent ultrasonic treatment for at least 30 min and cleaned in 75% (v/v) ethanol for 1 h. They were then put in the wells (one/well) and washed with the PBS solution (pH 7.4) thrice. After drying at room temperature, 3 mL of the poly-L-lysine solution (0.01% w/v) was added to each well and incubated for 1 h at 37 °C. After retrieval of the poly-L-lysine solution, the dried coverslips were used in subsequent experiments.

The MCF-7 breast cancer cells were seeded to the wells containing coverslips at 1×10^3 cells/well. After two days, the same volume of CS–SiO₂ HNPs conjugated with the antibody, blank CS–SiO₂ HNPs, and PBS solution were added to the wells. The final concentration of the nanospheres in the cell wells was controlled to within 0.1 and 0.5 μg/mL. After further incubation for 1 h, the solution was discarded. The cells were fixed with 3–5% glutaraldehyde (w/v, versus pH 7.4 PBS) after rinsing thoroughly thrice for at least 10 min each time. After discarding the fixative, ethanol solutions with different concentrations of 25%, 50%, 75%, 90%, and 100% were employed to dehydrate the cells after washing. Scanning electron microscopy (SEM) was used to observe the cells treated by the nanospheres after critical point drying (CPD) and gold coating.

2.10. In vivo therapy assay

The MCF-7 breast cancer cells were incubated under the aforementioned conditions and the harvested cells were adjusted to a concentration of 1×10^7 cells/mL. Nine 3-week old athymic nude mice (bought from Hubei Experimental Animal
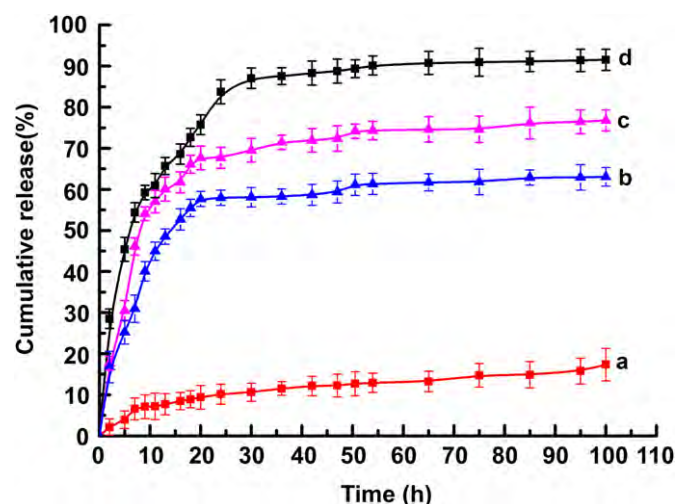

Fig. 3. Release profiles of BSA as one model protein drug from CS–SiO₂ and SiO₂ HNPs in the PBS media at different pH values: (a) CS–SiO₂ HNPs, pH 7.4, (b) SiO₂ HNPs, pH 7.4, (c) SiO₂ HNPs, pH 4.0, and (d) CS–SiO₂ HNPs, pH 4.0.
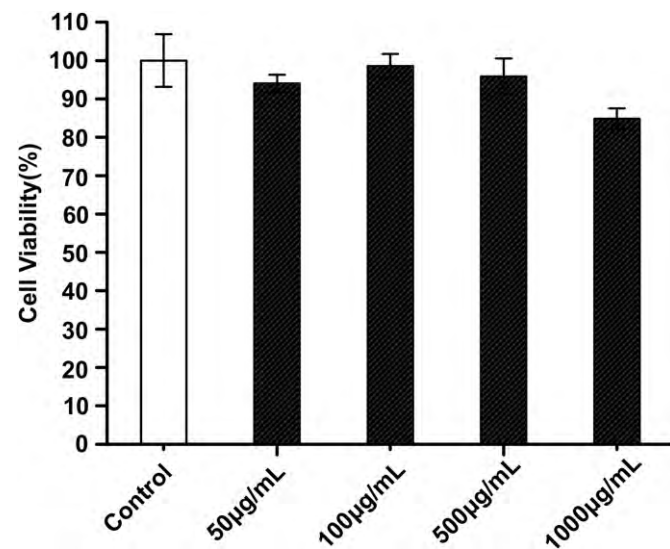

Fig. 4. In vitro cytotoxicity of CS–SiO₂ HNPs against MCF-7 cells after incubation for 48 h.
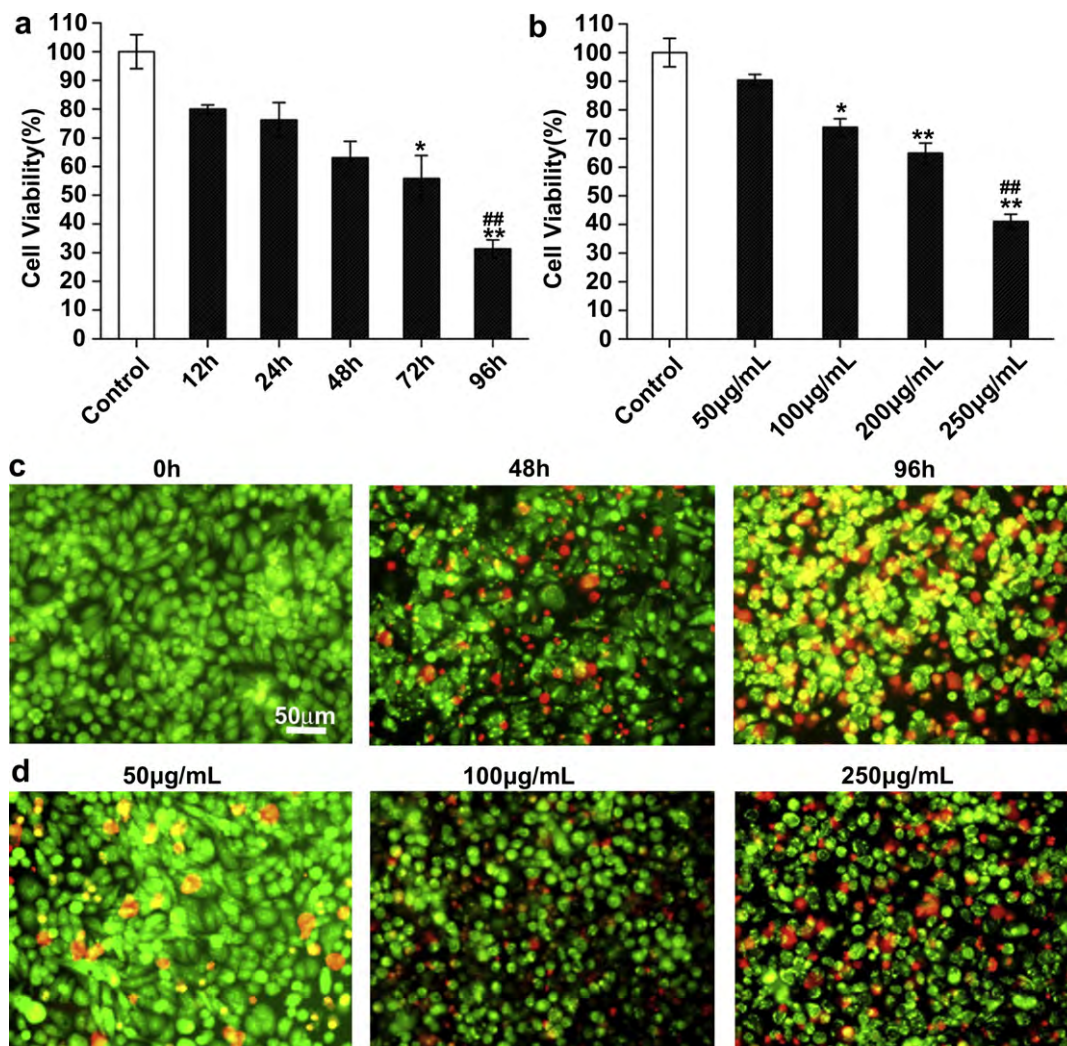
Fig. 5. Cytotoxicity of TNF-α-loaded CS–SiO₂ HNPs conjugated with the antibody against MCF-7 breast cancer cells incubated in a standard complete DMEM/F-12 medium containing 10% FBS (pH = 7.4): (a) Killing effects for different incubation time from 12 h to 96 h at the same concentrations (200 μg/mL of CS–SiO₂ HNPs containing about 500 ng/mL TNF-α). When the incubation time is increased to 72 h or 96 h, the nanocarriers exhibit higher cytotoxicity effect on MCF-7 cells than those incubated for 12 h ($^*P < 0.05$, $^{**}P < 0.01$ respectively), with significantly different cytotoxicity effects found between the 48 h and 96 h groups ($^{##}P\,0.01$); (b) Killing effects induced by gradient concentrations of agent nanocarriers from 50 to 250 μg/mL (the loaded TNF-α concentrations vary from 125 to 625 ng/mL) for the same incubation time of 48 h. Compared to the nanocarriers at a lower concentration of 50 μg/mL, those at 100, 200 and 250 μg/mL exhibit significantly higher killing potency to MCF-7 cells growth ($^*P < 0.05$ and $^{**}P < 0.01$, respectively). There is also significant difference in the killing effect between the 100 μg/mL and 250 μg/mL groups ($^{##}P\,0.01$); (c) The fluorescent photos of MCF-7 cells show the time-dependent effect of the nanocarriers (200 μg/mL of CS–SiO₂ HNPs loaded with about 500 ng/mL of TNF-α); (d) The concentration-dependent effect exhibited by the nanocarriers after 48 h. The scale bar is 50 μm in all images.

Research Center, China) were allowed to grow for one week before 1×10^6 MCF-7 breast cancer cells were injected subcutaneously into the right armpit. The mice were randomly divided into 3 groups after the average size of the tumors reached 30 mm³. The agents were injected into the three groups of mice according to the following protocol. For the control group (C group), 0.2 mL of PBS (pH 7.4) was injected intraperitoneally whereas for the nano group (N group), the solution consisting of the CS–SiO₂ HNPs, TNF-α, and antibody were injected with 0.2 mL of solution containing about 0.13 μg of TNF-α. For the TNF group (T group), the TNF-α agent (0.13 μg of TNF-α in 0.2 mL of PBS buffer solution) was administrated intraperitoneally only. The doses were administered once every two days. After two weeks, the mice were anaesthesized by injecting intraperitoneally 1.25% (w/v) avertin (Sigma) and the tumors from the three groups were taken out and weighed. All the animals were managed and treated according to the rules and regulations of the Institutional Animal Care and Use Committee at Hubei University, and the animal protocols were also approved by the Institutional Animal Care.

2.11. Characterization

The morphologies and sizes of the nanospheres (PS, SiO₂ HNPs and CS–SiO₂ HNPs) were examined by transmission electron microscopy (TEM, FEI Tecnai G20, U.S.A. FEI Corp.). The dispersions were diluted with ethanol, treated ultrasonically at 25 °C for 15 min, and dried onto carbon-coated copper grids before examination. The

average diameter of the nanospheres was calculated by measuring more than 100 nanospheres in the TEM images.

Scanning electron microscopy (SEM, Philips XL30) was used to characterize the morphologies of PS, SiO₂ HNPs and CS–SiO₂ HNPs. The samples were diluted with ethanol, dried on a silica wafer, and sputter-coated with gold prior to examination. In order to examine the hollow structures in the samples, the SiO₂ HNPs were dehydrated and embedded in epoxy for microtome. The obtained ultrathin sections were then sputter-coated with gold, and the morphology of the SiO₂ HNPs was examined by SEM. The cell samples after treatment with the nanospheres were observed by SEM after critical point drying (CPD) and gold coating.

Energy dispersive X-ray spectroscopy (EDS) was conducted on a Philips XL30 SEM to determine the surface composition of the SiO₂ and CS–SiO₂ HNPs.

The average hydrodynamic diameters of the PS, SiO₂ HNPs, and CS–SiO₂ HNPs were measured by dynamic light scattering (DLS) on a Zetasizer Nano Series instrument produced by Malvern. The zeta potentials were also determined using the Zetasizer Nano Series.

The Brunauer−Emmett−Teller (BET) measurement was carried out to examine the surface area and pore size distribution of the SiO₂ HNPs. Nitrogen adsorption/desorption isotherms were acquired from the SiO₂ HNPs on an ASAP 2010 (Micromeritics Instruments, USA) nitrogen adsorption apparatus. The samples were degassed at 150 °C for several hours prior to the BET measurement. The specific surface area on the SiO₂ HNPs was determined by a multipoint BET method
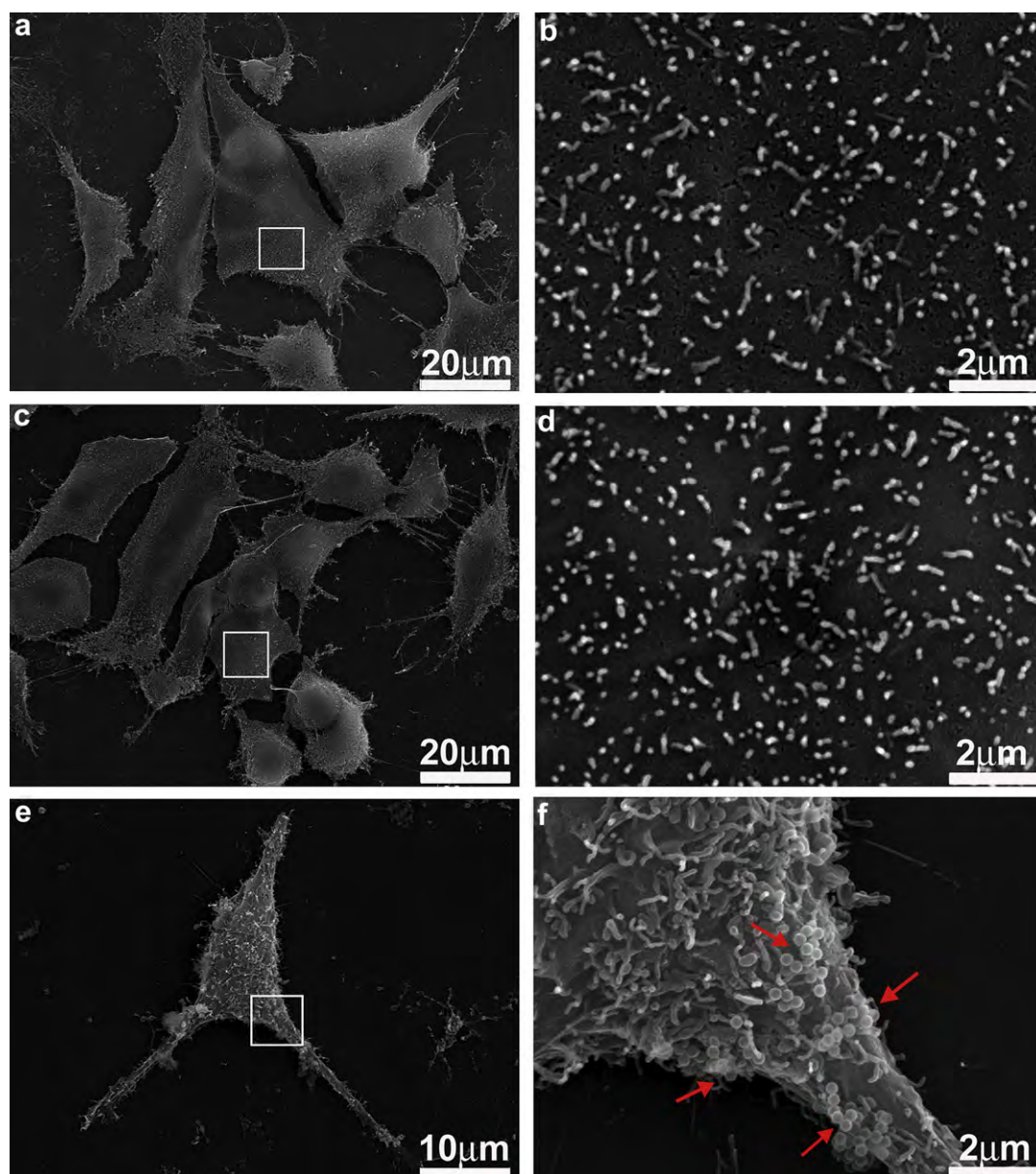
Fig. 6. SEM images showing the *in vitro* targeted MCF-7 breast cancer cells: (a, b) Blank control group without treatment with the nanospheres; (c, d) Control group treated with the CS—SiO₂ HNPs without the antibody; (e, f) Experimental group treated by the CS—SiO₂ HNPs conjugated with the antibody. The higher magnification SEM images in (b), (d) and (f) depict the selected area in (a), (c) and (e), respectively. The CS—SiO₂ HNPs conjugated with the antibody is located on the cell membrane (red arrows, f). The same concentration of blank CS—SiO₂ HNPs, and CS—SiO₂ HNPs conjugated with the antibody are used to treat the MCF-7 breast cancer cells in the wells, and all the cell samples are washed with the PBS solution several times before SEM observation. (For interpretation of the references to colour in this figure legend, the reader is referred to the web version of this article.).

according to the desorption data in the relative pressure P/P_0 range of 0.05—1 and the pore size distribution was calculated from the desorption isotherms using the BJH method.

UV—visible absorption spectra were obtained from the released BSA using UV—visible spectrophotometry (Hitachi UV-3000, Japan) at room temperature with the solution placed in a quartz cuvette.

Fluorescent microscopy was performed on the Olympus IX71 inverted microscope.

3. Results and discussion

3.1. Preparation and characterization of SiO₂ HNPs

The mono-dispersed cationic PS nanospheres are fabricated by emulsifier-free emulsion polymerization using PVP as the stabilizer and AIBA as the cationic initiator. The TEM image in Fig. 1a confirms that the cationic PS nanospheres are mono-dispersed and uniform on a large scale with an average diameter of about 216 nm (by averaging 100 particles in the TEM micrographs). The mono-dispersed cationic PS nanospheres are used as templates to fabricate the SiO₂ HNPs. After the cationic PS nanospheres are treated with TEOS and ammonia in ethanol at 50 °C for 1.5 h, the formed nanospheres are examined by TEM. As shown in Fig. 1b, most of mono-dispersed SiO₂ HNPs have interior cavities formed in the same medium during the sol—gel reaction process. The average size of the SiO₂ HNPs is about 236 nm. Comparing Fig. 1a and b, the high contrast between the inorganic shells and interior cavities illustrates that the templates of the cationic PS nanospheres are completely dissolved during the formation of the mono-dispersed
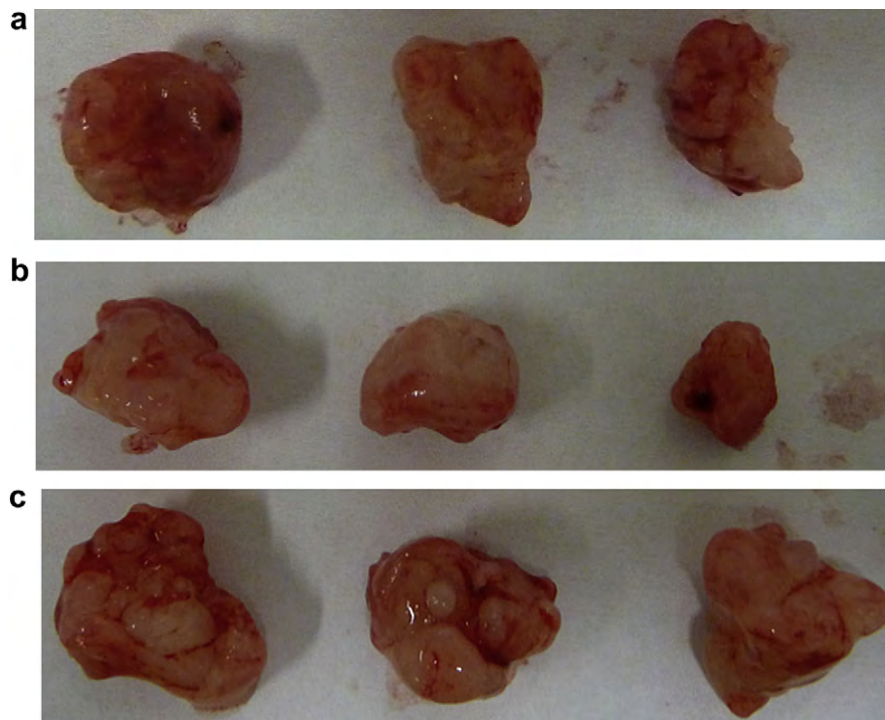
Fig. 7. Photos of tumors collected from mice in the three groups: (a) TNF group: only TNF-α agent was administered to the mice; (b) Nano group: nanocarriers composed of CS–SiO$_2$ HNPs, TNF-α and antibody were injected into the mice; (c) Control group: PBS (pH 7.4) was injected into the mice. The volume for injection is the same for all three groups and the total dosage of TNF-α per injection for the TNF group and Nano group is the same.
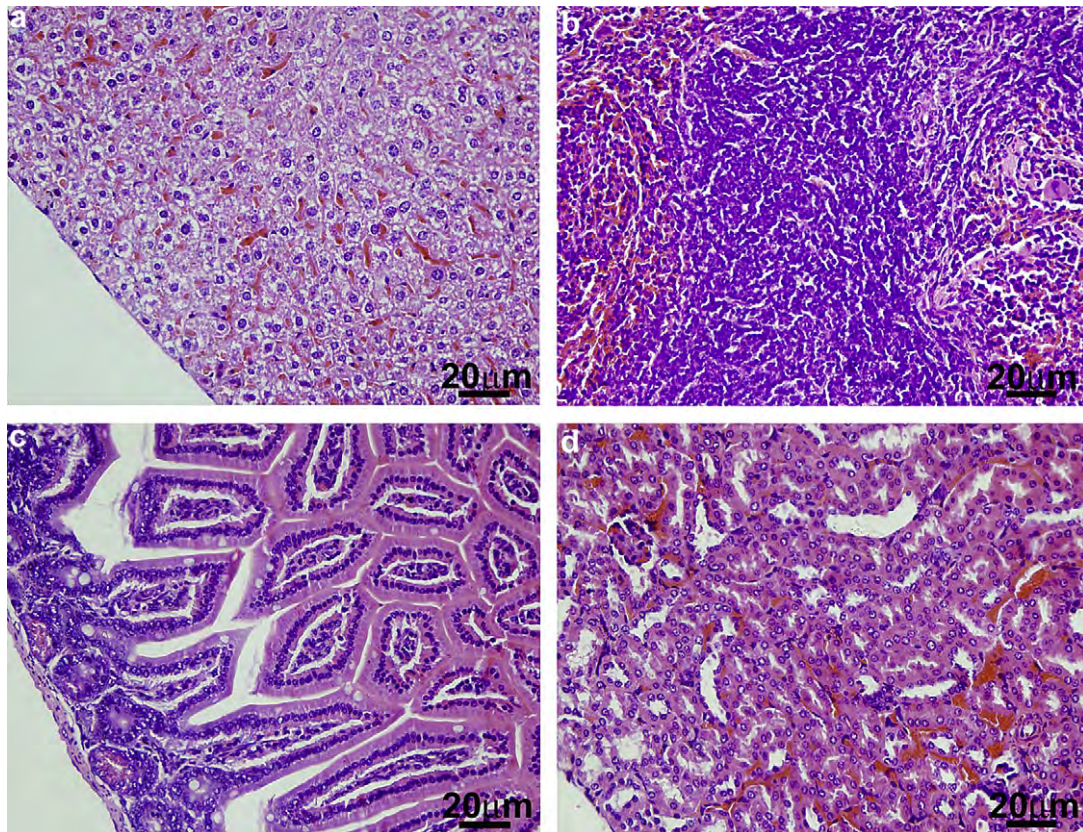

Fig. 8. Pathological inspection of the important viscera organs in the Nano group mice: (a) Liver; (b) Spleen, (c) Intestine, and (d) Kidney. No lymphocyte infiltration, necrosis, fibrosis, and other abnormal phenomena are observed. The scale bar is 20 μm in all the images.

SiO$_2$ HNPs. Hence, post-treatments such as additional organic solvent dissolution and calcination at elevated temperature are no longer necessary. The formation mechanism of the hollow nanospheres is described in our previous paper [27].

The SiO$_2$ HNPs are dehydrated, embedded in epoxy, microtomed, and examined by SEM. Fig. 1c reveals some broken SiO$_2$ nanospheres which confirm the hollow structure of the SiO$_2$ nanospheres. The porosity of the SiO$_2$ HNPs is studied by measuring the nitrogen adsorption–desorption isotherms and BET surface area. Fig. 1d depicts the N$_2$ adsorption–desorption isotherm and the pore size distribution (inset in Fig. 1d). The BET specific surface area is calculated to be 210.25 m^2 g^{-1}. The isotherms can be classified as type IV with an apparent hysteresis loop in the range of 0.5–1.0 P/P$_0$ indicating the presence of mesoporous structures in the SiO$_2$ HNPs. The Barrett–Joyner–Halenda (BJH) pore size distribution curve (inset in Fig. 1d) shows that the small pores are around 27.1 nm. These mesopores arise from the interspace among particles. Other macropores which are about 52.7 nm can be attributed to some broken SiO$_2$ HNPs. The presence of pores enable good connection with the interior cavity of the SiO$_2$ HNPs and provide the channels for drug penetration enabling storage inside the cavity and release to the surrounding medium at a later stage.

3.2. Preparation and characterization of CS–SiO$_2$ HNPs

Chitosan is used to decorate the surface of SiO$_2$ HNPs and produce a pH sensitive polyelectrolyte layer. In the process illustrated in Scheme 1, (3-Glycidyloxypropyl) trimethoxysilane (GPTMS) is first used to modify the SiO$_2$ HNPs in an acidic ethanol medium in which GPTMS reacts with the silanol groups on the SiO$_2$ surface via the formation of Si–O–Si bonds. The chitosan solution is then added to accomplish cross-linking on the surface of the SiO$_2$ HNPs [32,36].

The morphology of the SiO$_2$ HNPs before and after putting on the chitosan layer is examined by TEM and SEM. Fig. 2b and d discloses mono-dispersed CS–SiO$_2$ HNPs with an average size of 255 nm which is larger than that of the SiO$_2$ HNPs (Fig. 2a and c). The shell thickness increases significantly after introducing the chitosan coating. EDS shows Si and O with high intensity but less C is observed from the SiO$_2$ HNPs (Fig. 2e). The difference in the C signal indirectly demonstrates successful coating of chitosan (Fig. 2f). The dynamic light scattering (DLS) and zeta potential are also utilized to analyze the hollow nanospheres (Table 1). The hydrodynamic diameters (D$_h$) of SiO$_2$ and CS–SiO$_2$ HNPs determined from the DLS measurement are 242.8 and 263.7 nm, respectively and close to the average diameter derived from the TEM images. The zeta potential measurement shows that the SiO$_2$ HNPs have a negative potential of about −35 mV whereas the zeta potential of the CS–SiO$_2$ HNPs increases to +24.7 mV due to the cationic polysaccharide-chitosan decoration. All of these results corroborate that chitosan has been successfully introduced to the SiO$_2$ HNPs.

3.3. pH-controlled BSA protein release from CS–SiO$_2$ HNPs

To investigate the pH-dependent release of the loaded drug from CS–SiO$_2$ HNPs, BSA is used as a model protein (drug). The release studies are conducted in PBS buffer solutions at pH values of 7.4 and pH 4.0, respectively and the in vitro release profiles are displayed in Fig. 3. When BSA is loaded onto the CS–SiO$_2$ HNPs in the acidic PBS buffer solution (pH 4.0), rapid release (83.7% within 24 h) is observed from Fig. 3d. In comparison, at a pH of 7.4, only 17.4% of the BSA is released in the first 100 h (Fig. 3a). When SiO$_2$ HNPs are used as the nanocarriers (Fig. 3b and c), 58% and 67.7% of

the BSA are released in 24 h from the BSA loaded SiO$_2$ HNPs at pH values of 7.4 and 4.0, respectively. The results also illustrate that the amount of BSA released from the SiO$_2$ HNPs is smaller than that from the CS–SiO$_2$ HNPs at a pH of 4.0. It is because the BSA molecules are not only encapsulated inside the hollow nanospheres, but also absorbed by the chitosan layers due to the positive charges and amino functional groups on the surface [43].

The different BSA release behavior at different pH values can be attributed to the collapse and swelling of the chitosan layers on the surface of the SiO$_2$ HNPs. Under acidic conditions, the chitosan polymer chains become positively charged with the protonated amino groups. The positively charged chitosan chains swell opening the pores of the CS–SiO$_2$ HNPs. Consequently, the loaded BSA is released from the nanocarriers. On the contrary, at a neutral pH of 7.4, the chitosan polymer chains are deprotonated and collapse to form shielding layers on the porous surface of the SiO$_2$ HNPs. They thus block and restrict the release of BSA from the hollow interiors. The results demonstrate that chitosan plays an important role in the release mechanism stimulated by changes in the pH and after introduction of chitosan, the SiO$_2$ HNPs can offer pH sensitive, controlled release of drugs in the physiological environment.

3.4. In vitro cytotoxicity of CS–SiO$_2$ HNPs

The in vitro cytotoxicity of the CS–SiO$_2$ HNPs is evaluated referenced to MCF-7 breast cancer cells using the MTT assay. As shown in Fig. 4, the blank CS–SiO$_2$ HNPs do not show significant cytotoxicity against the MCF-7 cells. More than 84.9% of the cells are still viable even at a high concentration of CS–SiO$_2$ HNPs of 1000 μg/mL after incubation for 48 h. The results indicate that CS–SiO$_2$ HNPs have good cytocompatibility as nanocarriers.

3.5. In vitro killing potency

The drug nanocarriers are composed of CS–SiO$_2$ HNPs, antibody (signal recognition moiety), and TNF-α (killing-moiety) as illustrated in Scheme 1. To examine the in vitro killing potency, MCF-7 breast cancer cells are used. It is well known that TNF-α has the specific ability to bind to tumor necrosis factor receptors (TNFR) located at the cytoplasmic membrane of MCF-7 breast cancer cells [44]. Moreover, binding of TNF-α with TNFR can activate the apoptosis signal transmitting pathways cascade [45] by which TNF-α as a drug can suppress MCF-7 breast cancer cell growth and even kill them. When the drug nanocarrier solutions (200 μg/mL of CS–SiO$_2$ HNPs loaded with about 500 ng/mL of TNF-α) are used to treat MCF-7 breast cancer cells for different time periods, the cytotoxicity is observed to increase with time (Fig. 5a). After 96 h, the nanospheres exhibit the higher growth inhibition effect on the breast cancer cells compared to those incubated for shorter time (12 h or 24 h) ($^{**}P < 0.01$). The increased cytotoxicity probably results from sustained release of the encapsulated TNF-α from the CS–SiO$_2$ HNPs after a long incubation time. Fluorescent microscopy provides more evidence of the time-dependent killing phenomenon. As shown in Fig. 5c, no killing can be found from all the plates (green color) when the drug nanocarriers are administered to MCF-7 breast cells at 0 h. However, after incubation for 48 h and 96 h, more MCF-7 breast cancer cells are killed (red color). In addition, both the cytotoxicity and fluorescent results demonstrate that the drug nanocarriers exhibit a concentration-dependent cytotoxicity effect. When the amounts of the injected nanocarriers increase from 50 to 250 μg/mL (loaded TNF-α with concentrations from 125 to 625 ng/mL), the MCF-7 breast cancer cells are gradually killed and the number of dead cells (red color) goes up after incubation for 48 h (Fig. 5b and d). (For interpretation of the references to

colour in this figure legend, the reader is referred to the web version of this article.)".

During drug delivery, the signal recognition moiety- antibody (to ErbB 2, ab2428) on the CS–SiO$_2$ HNPs can bind to the antigen ErbB 2 on the cell membrane of the MCF-7 breast cancer cells. This helps the nanocarriers to aggregate on the cell membranes. It should be noted that the drug delivery system described here is very different from other carriers that deliver genes or other anti-cancer therapeutic agents such as Paclitaxel and Doxorubicin to cancerous cells. The latter must not only successfully transfer onto the targeted cells, but also deliver the genes or anticancer drugs in order to express the viability on the cytoplasm or nuclei of the targeted cells [18,46,47]. However, TNF-α does not necessarily need to be transferred to the cells to express its efficacy. The destination of the nanocarriers is the space in the vicinity of the membranes of the MCF-7 breast cancer cells and it can be reached by the inter-action between the antibody and ErbB 2 epitope. The released TNF-α can bind to the tumor necrosis factor receptor (TNFR) to activate the apoptosis signal transmitting pathways cascade suppressing the growth of the MCF-7 breast cancer cells and killing them effi-ciently [44,45]. Therefore, the multifunctional nanocarriers composed of signal recognition, killing-moiety components, and pH-sensitive polymer layers can offer high killing potency via tar-geted delivery and controlled release of drugs against cancerous cells.

3.6. In vitro targeting

To further examine and demonstrate that the CS–SiO$_2$ HNPs conjugated with antibody molecules can target MCF-7 breast cancer cells, SEM is conducted after the cells are treated with the CS–SiO$_2$ HNPs conjugated with/without the antibody. As shown in Fig. 6e and f, the CS–SiO$_2$ HNPs conjugated to the antibody can bind to the cell membrane even after washing (shown by red arrows in Fig. 6f). It may be because the antibody molecules on the CS–SiO$_2$ HNPs have the ability to bind to the antigen ErbB 2 on the cell membranes of the MCF-7 breast cancer cells [44]. Therefore, the CS–SiO$_2$ HNPs located at the cell membranes of the targeted cells can help keep the local TNF-α concentration higher thereby increasing the binding efficacy of the TNF-α to the receptors.

Although the CS–SiO$_2$ HNPs have a positively charged surface, the SEM images in Fig. 6c and d illustrate no obvious presence of the nanospheres on the surface of the MCF-7 cell membranes compared to Fig. 6e and f when the CS–SiO$_2$ HNPs without the antibody molecules are used to treat the cells in the control experiments. It can be inferred that the electrostatic interaction between the CS–SiO$_2$ HNPs and cell membranes is not strong enough to keep the nanospheres on the membrane surface, and so the nanospheres can be removed from the cell surface after washing. Moreover, some of CS–SiO$_2$ HNPs may be internalized by MCF-7 breast cancer cells because the probability of endocytosis on these nanospheres cannot be eliminated in cells [48]. However, the TNF-α protein molecule as an anticancer drug can only bind to the tumor necrosis factor receptor (TNFR) on the cell membrane to activate the downstream signal molecules and induce the apoptosis of target cells [44]. Therefore, endocytosis can influence the efficacy of the CS–SiO$_2$ HNPs conjugated to the antibody to some extent but not excessively, and it will be confirmed by other in vitro and in vivo experiments described later.

3.7. In vivo anti-tumor effect

During the in vivo breast cancer therapy experiments on animal models, the weight of all the mice is quite stable and no abnor-mality is observed (data not shown). The drugs are intraperitoneally administered to the mice once every two days. After two weeks, no mice die and the tumors collected from three groups are weighed. As shown in Fig. 7, when only the TNF-α agent is intraperitoneally administered to the mice, the total weight of the tumors in the TNF group (Fig. 7a) is nearly 90% of that in the control group (Fig. 7c). However, the total weight of the tumors from the Nano group (Fig. 7b) is about 45% of that of the Control group (Fig. 7c) and is smaller than that of the TNF group (Fig. 7a). The results demonstrate that TNF-α loaded on the CS–SiO$_2$ HNPs can effectively suppress tumor growth compared to when only TNF-α is administered. The enhanced tumor growth inhibition observed from the Nano group is believed to stem from sustained TNF-α release from the CS–SiO$_2$ HNPs in vivo as well as accumulation of the drug nanocarriers inside the tumor micro-environment. The nanocarriers can penetrate the microcirculation system of the solid tumors into the extracellular matrix (ECM) through the recognition between antibody on the CS–SiO$_2$ HNPs and antigen-ErbB 2 epitope on the MCF-7 cancer cell membranes. Hence, the nano-carriers aggregate on the membrane of the MCF-7 breast cancer cells. Owing to the acidic local environment around the cancerous cells, the chitosan chains on the drug nanocarriers swell and the pores of the CS–SiO$_2$ HNPs are opened. Consequently, the loaded TNF-α is released from the CS–SiO$_2$ HNPs making the TNF-α concentration around the cell membrane higher than that in other areas. With the released TNF-α binding to the tumor necrosis factor receptor (TNFR), the apoptosis signal transmitting pathways cascade is activated further enhancing the tumor suppression effect. However, when only the TNF-α protein molecules are administered to the TNF group, the killing efficacy diminishes. It may be because the TNF-α protein molecules cannot persistently stay inside the core area of the solid tumors due to abnormal vasculature [49]. Furthermore, the amount of TNF-α entering the core area of the solid tumors is not as much as that of the nano-carriers. We have also studied the bio-safety of the nanocarriers composed of CS–SiO$_2$ HNPs, TNF-α, and antibody in vivo (Fig. 8). No inflammation and leukocyte infiltration abnormality can be observed from our pathological study of the viscera organs including liver, spleen, intestine, and kidney.

4. Conclusion

Mono-dispersed and pH-sensitive CS–SiO$_2$ HNPs are prepared by introducing chitosan onto SiO$_2$ HNPs. The cationic poly-saccharide-chitosan introduces a pH sensitive polyelectrolyte layer on the SiO$_2$ HNPs. After conjugating the antibody (to ErbB 2) to CS–SiO$_2$ HNPs, the nanocarriers exhibit good performance in delivering TNF-α to breast cancer cells both in vitro and in vivo. The in vitro results confirm that the high affinity between the antibody and antigen can direct the CS–SiO$_2$ HNPs to retain the space close to the MCF-7 breast cancer cell membrane, thus achieving targeted delivery to cancer cells. On account of the acidic micro-environ-ment inside solid tumors, the loaded TNF-α can gradually be released from the nanocarriers, bind TNFR to activate the down-stream signal molecules, and induce apoptosis of targeted cells. Our results indicate that the mono-dispersed pH sensitive CS–SiO$_2$ HNPs are promising drug nanocarriers in high-efficiency cancer therapy. Our research also provides insight to the understanding of SiO$_2$-based nanomaterials and their applications to nanomedicine.

References

[1] Ferrari M. Cancer nanotechnology: opportunities and challenges. Nat Rev Cancer 2005;5:161–71.

[2] Jones D. Cancer nanotechnology: small, but heading for the big time. Nat Rev Drug Discov 2007;6:174–5.

[3] Peer D, Karp JM, Hong S, FaroKhzad OC, Margalit R, Langer R. Nanocarriers as an emerging platform for cancer therapy. Nat Nanotechnol 2007;2:751–60.

[4] West JL, Halas NJ. Engineered nanomaterials for biophotonics applications: improving sensing, imaging, and therapeutics. Annu Rev Biomed Eng 2003; 5:285–92.

[5] Lee JH, Huh YM, Jun Y, Seo J, Jang J, Song HT, et al. Artificially engineered magnetic nanoparticles for ultra-sensitive molecular imaging. Nat Med 2007; 13:95–9.

[6] Quintana A, Raczka E, Piehler L, Lee I, Myc A, Majoros I, et al. Design and function of a dendrimer-based therapeutic nanodevice targeted to tumor cells through the folate receptor. Pharm Res 2002;19:1310–6.

[7] El-Sayed IH, Huang XH, El-Sayed MA. Surface plasmon resonance scattering and absorption of anti-EGFR antibody conjugated gold nanoparticles in cancer diagnostics: applications in oral cancer. Nano Lett 2005;5:829–34.

[8] Poland CA, Duffin R, Kinloch I, Maynard A, Wallace WAH, Seaton A, et al. Carbon nanotubes introduced into the abdominal cavity of mice show asbestos-like pathogenicity in a pilot study. Nat Nanotechnol 2008;3:423–8.

[9] Huang XH, El-Sayed IH, Qian W, El-Sayed MA. Cancer cell imaging and photothermal therapy in the near-infrared region by using gold nanorods. J Am Chem Soc 2006;128:2115–20.

[10] Mal NK, Fujiwara M, Tanaka Y. Photocontrolled reversible release of guest molecules from coumarin-modified mesoporous silica. Nature 2003; 421:350–3.

[11] Gao XH, Cui YY, Levenson RM, Chung LWK, Nie SM. In vivo cancer targeting and imaging with semiconductor quantum dots. Nat Biotechnol 2004;22: 969–76.

[12] Yavuz MS, Cheng Y, Chen J, Cobley CM, Zhang Q, Rycenga M, et al. Gold nanocages covered by smart polymers for controlled release with near-infrared light. Nat Mater 2009;8:935–9.

[13] Zhu YF, Shi JL, Shen WH, Dong XP, Feng JW, Ruan ML, et al. Stimuli-responsive controlled drug release from a hollow mesoporous silica sphere/polyelectrolyte multilayer core-shell structure. Angew Chem Int Ed 2005;44:5083–7.

[14] Jiang XM, Ward TL, Cheng YS, Liu JW, Brinker CJ. Aerosol fabrication of hollow mesoporous silica nanoparticles and encapsulation of L-methionine as a candidate drug cargo. Chem Commun 2010;46:3019–21.

[15] Zhu YF, Shi JL, Shen WH, Chen HR, Dong XP, Ruan ML. Preparation of novel hollow mesoporous silica spheres and their sustained-release property. Nanotechnology 2005;16:2633–8.

[16] Botterhuis NE, Sun QY, Magusin P, van Santen RA, Sommerdijk N. Hollow silica spheres with an ordered pore structure and their application in controlled release studies. Chem Eur J 2006;12:1448–56.

[17] Yang J, Lee J, Kang J, Lee K, Suh JS, Yoon HG, et al. Hollow silica nanocontainers as drug delivery vehicles. Langmuir 2008;24:3417–21.

[18] Yan EY, Ding Y, Chen CJ, Li RT, Hu Y, Jiang XQ. Polymer/silica hybrid hollow nanospheres with pH-sensitive drug release in physiological and intracellular environments. Chem Commun; 2009:2718–20.

[19] Lay CL, Liu HQ, Wu DC, Liu Y. Poly(ethylene glycol)-graft-hollow silica vesicles for drug delivery. Chem Eur J 2010;16:3001–4.

[20] Kim J, Kim HS, Lee N, Kim T, Kim H, Yu T, et al. Multifunctional uniform nanoparticles composed of a magnetite nanocrystal core and a mesoporous silica shell for magnetic resonance and fluorescenceimaging and for drug delivery. Angew Chem Int Ed 2008;47:8438–41.

[21] Zhu J, Tang JW, Zhao LZ, Zhou XF, Wang YH, Yu CZ. Ultrasmall, well-dispersed, hollow siliceous spheres with enhanced endocytosis properties. Small 2010; 6:276–82.

[22] Lu Y, Fan H, Stump A, Ward TL, Rieker T, Brinker CJ. Aerosol-assisted self-assembly of mesostructured spherical nanoparticles. Nature 1999;398:223–6.

[23] Nagao D, van Kats CM, Hayasaka K, Sugimoto M, Konno M, Imhof A, et al. Synthesis of hollow asymmetrical silica dumbbells with a movable inner core. Langmuir 2010;26:5208–12.

[24] Tissot I, Reymond JP, Lefebvre F, Bourgeat-Lami E. SiOH-functionalized polystyrene latexes. A step toward the synthesis of hollow silica nanoparticles. Chem Mater 2002;14:1325–31.

[25] Lu Y, McLellan J, Xia YN. Synthesis and crystallization of hybrid spherical colloids composed of polystyrene cores and silica shells. Langmuir 2004; 20:3464–70.

[26] Caruso F, Caruso RA, Mohwald H. Nanoengineering of inorganic and hybrid hollow spheres by colloidal templating. Science 1998;282:1111–4.

[27] Deng ZW, Chen M, Zhou SX, You B, Wu LM. A novel method for the fabrication of monodisperse hollow silica spheres. Langmuir 2006;22:6403–7.

[28] Shi J, Votruba AR, Farokhzad OC, Langer R. Nanotechnology in drug delivery and tissue engineering: from discovery to applications. Nano Lett 2010; 10:3223–30.

[29] Farokhzad OC, Langer R. Impact of nanotechnology on drug delivery. ACS Nano 2009;3:16–20.

[30] Bhattarai N, Gunn J, Zhang MQ. Chitosan-based hydrogels for controlled, localized drug delivery. Adv Drug Deliv Rev 2010;62:83–99.

[31] Schuetz YB, Gurny R, Jordan O. A novel thermoresponsive hydrogel based on chitosan. Eur J Pharm Biopharm 2008;68:19–25.

[32] Wu J, Sailor M. Chitosan hydrogel-capped porous SiO_2 as a pH responsive nano-valve for triggered release of insulin. Adv Funct Mater 2009;19:733–41.

[33] Yang Q, Wang SH, Fan PW, Wang LF, Di Y, Lin KF, et al. pH-responsive carrier system based on carboxylic acid modified mesoporous silica and polyelectrolyte for drug delivery. Chem Mater 2005;17:5999–6003.

[34] Thistlethwaite AJ, Leeper DB, Moylan Iii DJ, Nerlinger RE. pH distribution in human tumors. Int J Radiat Oncol Biol Phys 1985;11:1647–52.

[35] Kallinowski F, Vaupel P. pH distributions in spontaneous and isotransplanted rat tumours. Br J Cancer 1988;58:314–21.

[36] Liu YL, Su YH, Lai JY. In situ crosslinking of chitosan and formation of chitosan-silica hybrid membranes with using gamma-glycidoxypropyltrimethoxysilane as a crosslinking agent. Polymer 2004;45:6831–7.

[37] Zhu Y, Fang Y, Kaskel S. Folate-conjugated $Fe_3O_4@SiO_2$ hollow mesoporous spheres for targeted anticancer drug delivery. J Phys Chem C 2010; 114:16382–8.

[38] Brouckaert PGG, Leroux-Roels GG, Guisez Y, Tavernier J, Fiers W. In vivo anti-tumour activity of recombinant human and murine TNF, alone and in combination with murine IFN-γ, on a syngeneic murine melanoma. Int J Cancer 1986;38:763–9.

[39] Balkwill FR, Lee A, Aldam G, Moodie E, Thomas JA, Tavernier J, et al. Human-tumor xenografts treated with recombinant human-tumor necrosis factor alone or in combination with interferons. Cancer Res 1986;46:3990–3.

[40] Sugarman BJ, Aggarwal BB, Hass PE, Figari IS, Palladino MA, Shepard HM. Recombinant human-tumor necrosis factor-alpha:effects on proliferation of normal and transformed cells in vitro. Science 1985;230:943–5.

[41] Mansur HS, Oréfice RL, Vasconcelos WL, Lobato ZP, Machado LJC. Biomaterial with chemically engineered surface for protein immobilization. J Mater Sci Mater Med 2005;16:333–40.

[42] Cai WY, Gentle IR, Lu GQ, Zhu JJ, Yu AM. Mesoporous silica templated biolabels with releasable fluorophores for immunnoassays. Anal Chem 2008;80: 5401–6.

[43] Song SW, Hidajat K, Kawi S. pH-controllable drug release using hydrogel encapsulated mesoporous silica. Chem Commun; 2007:4396–8.

[44] Hueber AO. Role of membrane microdomain rafts in TNFR-mediated signal transduction. Cell Death Differ 2003;10:7–9.

[45] Balkwill F. Tumour necrosis factor and cancer. Nat Rev Cancer 2009; 9:361–71.

[46] Akita H, Harashima H. Advances in non-viral gene delivery: using multifunctional envelope-type nano-device. Expert Opin Drug Delivery 2008;5:847–59.

[47] Cheng K, Peng S, Xu CJ, Sun SH. Porous hollow Fe_3O_4 nanoparticles for targeted delivery and controlled release of cisplatin. J Am Chem Soc 2009; 131:10637–44.

[48] Petros RA, DeSimone JM. Strategies in the design of nanoparticles for therapeutic applications. Nat Rev Drug Discov 2010;9:615–27.

[49] Minchinton AI, Tannock IF. Drug penetration in solid tumours. Nat Rev Cancer 2006;6:583–92.